Analysis of Circuit for Dynamic Wireless Power Transfer by Stepping Stone System

Hiroshi Uno [1] Jun Yamada[1] Yasuyoshi Kaneko [1] Toshiyuki Fujita [2] Hiroyuki Kishi [2]

1) Saitama University, Graduate school of Science and Engineering,

255 Shimo-Okubo, Sakura-ku, Saitama-shi, Saitama, 338-8570, Japan (E-mail: h.uno.418@ms.saitama-u.ac.jp)

2) Technova Inc.,

13th Fl. The Imperial Hotel Tower, 1-1 Uchisaiwai-cho, 1-chome, Chiyoda-ku, Tokyo, 100-0011, Japan

Presented at EVS 31 & EVTeC 2018, Kobe, Japan, October 1 - 3, 2018

ABSTRACT: Electric Vehicles (EVs) has risen to prominence as a research topic due to contemporary environmental concerns and the resultant need for energy conservation. One of the challenges in designing EVs is extending their cruising distance. An approach to address this problem is dynamic wireless power transfer. This paper aims to provide a really simple model dynamic wireless power transfer system. Specific attention is given to verifying the coupling coefficient when the secondary coil is misaligned. The model is used to analyze voltage and current characteristics in two different in two topologies, series-series (SS) and parallel–series (PS). Findings are tested validated via a simulation and an experiment.

KEY WORDS: Wireless Power Transfer, Dynamic Wireless Power Transfer, Circuit Topology

1. INTRODUCTION

Contemporary environmental concerns and the resultant need for energy conservation has highlighted electric vehicles (EVs) as one of cars worthy of siginificant research focus. One of the biggest problems presented by EVs is that the cruising distance is shorter and fueling time is longer than that of a car powered by fuels. Dynamic wireless power transfer (DWPT)[(1)] is proposed as a method for solving these problems. Two main approaches exist, namely the loop coll approach[(2)], and the location with spacing approach[(1)(3)(4)(5)], within which there are specific different methods. This paper draws on “the stepping stone system” method proposed in references (1) and (3). Compared with the loop coil method, “the stepping stone system” is expected to be cheaper and easier to implement, in terms of the laying of the ground coils[(1)]. Proposed DWPT circuit topologies in “the stepping stone system” are series-series (SS) and parallel-series (PS). The SS topology is one of the most common circuit topologies used to implement wireless power transfer (WPT). Previous studies used this topology for constant current[(1)], power supply, in the repeater coil method[(3)], for comparison with a stationary system[(4)]. With respect to the PS topology, one of the characteristics is that the input impedance approaches infinity when the secondary side of the topology is absent. DWPT is proposed to take advantage of this characteristic[(5)]. Very few previous works have analyzed both topologies including variable voltage and current by misalignment of running direction; if all possible phenomena are included, the analysis becomes complicated and it is very difficult to make any predictions.

In this paper, the aim is to construct as simple a model of a DWPT system as possible. This paper focuses on the verification of the coupling coefficient when the secondary coil is misaligned, providing insight into the common tendency of voltage and current fluctuation in such circuits. Two topologies are analyzed: series SS topology, specifically a series connection of primary coils connected in series to resonant capacitors, and parallel PS topology, specifically the parallel connection of primary coils connected in parallel to resonant capacitors, with two primary coils and a secondary coil. These topological approaches are validated via an electrical circuit simulator and via an experiment.

The structure of this paper is as follows. Section 2 gives an overview of the SS and PS topologies as this applies to a primary

coil and a secondary coil. Section 3 provides results and analysis of input and output data for voltage, current and output power using the series SS and parallel PS topologies and considering misalignment in the running direction, and describes relevant features. Section 4 details the circuit simulator, and Section 5 describes the result of the experiment. Finally, Section 6 summarizes the research and presents conclusions.

2. Circuit topology of a primary coil and a secondary coil

This section examines basic characteristic of the SS and PS topologies using a primary and secondary coil. In this paper, wind resistance is much smaller than reactance at the resonant frequency. Moreover, the input of square wave voltage for actual applications has little influence on the higher harmonics of current because WPT is a resonant circuit. Therefore, only the root mean square (RMS) of the fundamental wave component is considered.

2.1. SS topology

This section describes the SS topology, which, as previously mentioned, is one of the most widely used in WPT. A circuit diagram with an SS topology is shown in Fig. 1.

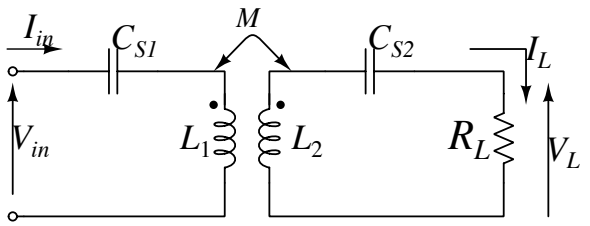

Fig.1 SS topology

In this circuit, for resonant capacitors C_{s1}, C_{s2} ,

$$C_{s1}=\frac{1}{\omega^2 L_1}, C_{s2}=\frac{1}{\omega^2 L_2}, \tag{1}$$

where the input and output characteristics are given by

$$\begin{pmatrix} V_{in} \\ I_{in} \end{pmatrix}=\begin{pmatrix} 0 & -j\omega M \\ \frac{1}{j\omega M} & 0 \end{pmatrix}\begin{pmatrix} V_L \\ I_L \end{pmatrix}=\begin{pmatrix} 0 & -j\omega k\sqrt{L_1 L_2} \\ \frac{1}{j\omega k\sqrt{L_1 L_2}} & 0 \end{pmatrix}\begin{pmatrix} V_L \\ I_L \end{pmatrix}, \tag{2}$$

and the input impedance is given by

$$Z_{in}=\frac{(\omega M)^2}{R_L}=\frac{(\omega k)^2 L_1 L_2}{R_L}\ . \tag{3}$$

From Eq. (2), the SS topology has immittance converter[6] which outputs a constant current when input remains at a constant voltage. From Eq. (3), when the coupling coefficient k decreases due to misalignment of the secondary coil, input impedance approaches zero.

2.2. PS topology

This section describes the PS topology, shown in Fig. 2.

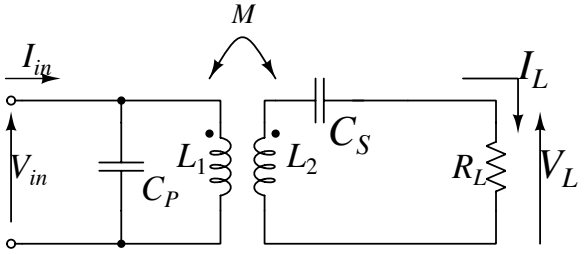

Fig.2 PS topology

In the figure shown in this figure, for resonant capacitors, C_P, C_s,

$$C_p=\frac{1}{\omega^2 L_1}, C_s=\frac{L_1}{\omega^2\left(L_1 L_2-M^2\right)}=\frac{1}{\omega^2 L_2\left(1-k^2\right)}, \tag{4}$$

where the input and output characteristics are given by

$$\begin{pmatrix} V_{in} \\ I_{in} \end{pmatrix}=\begin{pmatrix} \frac{L_1}{M} & 0 \\ 0 & \frac{M}{L_1} \end{pmatrix}\begin{pmatrix} V_L \\ I_L \end{pmatrix}=\begin{pmatrix} \frac{1}{k}\sqrt{\frac{L_1}{L_2}} & 0 \\ 0 & k\sqrt{\frac{L_2}{L_1}} \end{pmatrix}\begin{pmatrix} V_L \\ I_L \end{pmatrix}, \tag{5}$$

and input impedance is given by

$$Z_{in}=\left(\frac{L_1}{M}\right)^2 R_L=\frac{1}{k^2}\frac{L_1}{L_2}R_L\,. \tag{6}$$

From Eq. (5), the PS topology has the ideal transformer which outputs a constant voltage when input remains at a constant voltage. If the primary coil and secondary coil have the same shape, $\sqrt{L_1/L_2}$ is the turn ratio between the primary side and the secondary side. It is necessary to increase the number of turns on the secondary side when taking voltage and current at the same ratio as the primary side, because the coefficient coupling k causes secondary self-inductance. From Eq. (6), when the coupling coefficient k decreases due to misalignment of the secondary coil, input impedance approaches infinity. The PS topology enables the performance of passive switching.

3. Analysis of circuit topology for two primary coils and a secondary coil

Fig. 3 shows the series SS topology circuit, and Fig. 4 shows the parallel PS topology circuit.

Table 1. The voltage and current characteristics for constant input voltage

	Series SS topology	Parallel PS topology
V_{in}	Constant	Constant
I_{in}	$\frac{R_L}{(k_{13}+k_{23})^2\omega^2 LL_3}V_{in}$	$\frac{L_3}{L}\frac{(k_{13}+k_{23})^2}{R_L+j(\kappa-k_{13}^2-k_{23}^2)\omega L_3}V_{in}$
V_L	$j\frac{R_L}{(k_{13}+k_{23})\omega\sqrt{LL_3}}V_{in}$	$\sqrt{\frac{L_3}{L}}\frac{(k_{13}+k_{23})R_L}{R_L+j(\kappa-k_{13}^2-k_{23}^2)\omega L_3}V_{in}$
I_L	$j\frac{V_{in}}{(k_{13}+k_{23})\omega\sqrt{LL_3}}$	$\sqrt{\frac{L_3}{L}}\frac{k_{13}+k_{23}}{R_L+j(\kappa-k_{13}^2-k_{23}^2)\omega L_3}V_{in}$
P_L	$\frac{R_L}{(k_{13}+k_{23})^2\omega^2 LL_3}V_{in}^2$	$\frac{L_3}{L}\frac{(k_{13}+k_{23})^2R_L}{R_L^2+(\kappa-k_{13}^2-k_{23}^2)^2\omega^2L_3^2}V_{in}^2$

Table 2. The voltage and current characteristics for constant input current

	Series SS topology	Parallel PS topology
V_{in}	$\frac{\omega^2(k_{13}+k_{23})^2LL_3}{R_L}I_{in}$	$\frac{L}{L_3}\frac{R_L+j(\kappa-k_{13}^2-k_{23}^2)\omega L_3}{(k_{13}+k_{23})^2}I_{in}$
I_{in}	Constant	Constant
V_L	$j\omega(k_{13}+k_{23})\sqrt{LL_3}I_{in}$	$\sqrt{\frac{L}{L_3}}\frac{R_L}{k_{13}+k_{23}}I_{in}$
I_L	$\frac{j\omega(k_{13}+k_{23})\sqrt{LL_3}}{R_L}I_{in}$	$\sqrt{\frac{L}{L_3}}\frac{I_{in}}{k_{13}+k_{23}}$
P_L	$\frac{\omega^2(k_{13}+k_{23})^2LL_3}{R_L}I_{in}^2$	$\frac{L}{L_3}\frac{R_LI_{in}^2}{(k_{13}+k_{23})^2}$

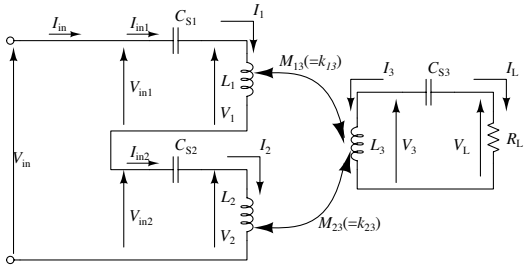

Fig.3 Series SS topology

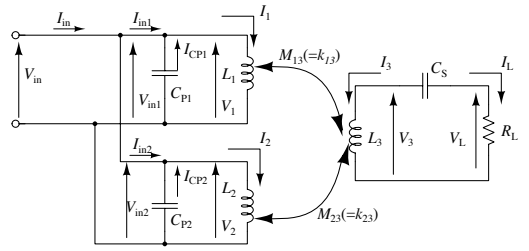

Fig.4 Parallel PS topology

In the circuit analysis of Figs. 3 and 4, the following conditions are taken into consideration for simplicity.

- When the separation between the primary coils is suitable, mutual coupling is ignored.
- Winding resistances are suitably smaller than reactances.
- All primary coils are the same shape and perform the same. (L=L_1=L_2)
- Resonant capacitors apply the resonance condition of inductances at the 0 mm point, and do not change on the way. (Fig. 5)

When applying the conditions, the capacitance in the series SS topology are determined as follows:

$$C_{S1}=C_{S2}=\frac{1}{\omega^2 L},C_{S3}=\frac{1}{\omega^2 L_3}, \quad (7)$$

and the capacitance in the parallel PS topology are determined as follows:

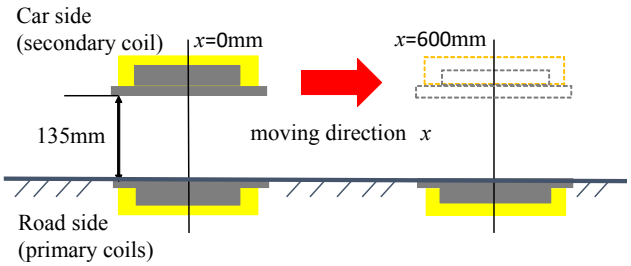

Fig.5 Pattern diagram

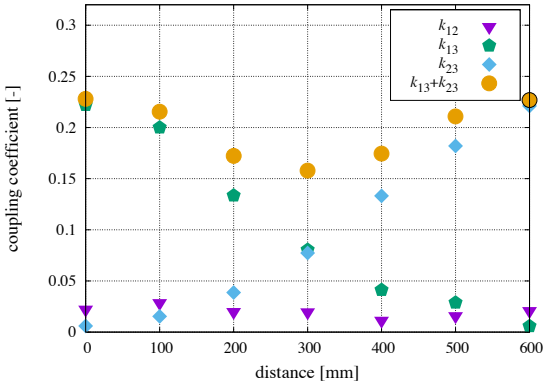

Fig.6 Variable coupling coeffient

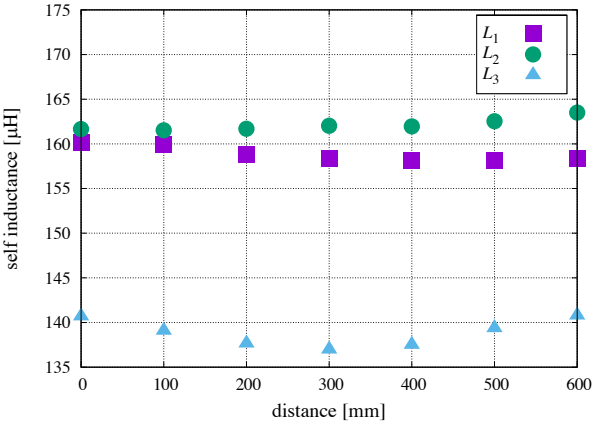

Fig.7 Variable self inductance

Table 3. Specifications of solenoid coils

Gap[mm]		135
Coil type		H-shaped core
Size[mm]	Ground side	320×446×31.5
	Vehicle side	270×270×21.5
Core Size[mm]	Ground side	300×420×20
	Vehicle side	250×250×10
Winding Size[mm]	Ground side	172×424×20
	Vehicle side	172×166×16.5
Winding[mm]	Ground side	20T×2p
	Vehicle side	22T×1p

$$C_{P1} = C_{P2} = \frac{1}{\omega^2 L}, C_S = \frac{1}{\omega^2 (1-\kappa) L_3}, \quad (8)$$

where κ represents the coupling coefficient $k_{13}^2+k_{23}^2$ at the 0 mm point setting on the secondary side. Tables 1 and 2 list the voltage and current characteristics for constant input voltage, and constant input current, respectively. From Tables 1 and 2, the sum of coupling coefficients k_{13}, k_{23} shows a large fluctuation on voltage and current. For example, when $k_{13}+k_{23}$ decreases, the value increases if this parameter is the numerator, and when $k_{13}+k_{23}$ decreases, the value increases if this parameter is the denominator. Furthermore, the parallel PS topology has a bigger misalignment influence than the series SS topology because an imaginary component appears in the equations in this topology when the secondary coil moves from the 0 mm point.

4. Simulation

The simulation is run using by PSIM, a circuit simulator, to validate the equations presented in Section 3.The coils uses an H-shaped solenoid, which has high misalignment performance[7]. The coil shape parameters are listed in Table 3. In this paper, the value obtained by actually measuring the constant of the coil at intervals of 100 mm between 0 and 600 mm was used. The coil parameters obtained by measurement are given in Figs. 6 and 7. Moreover, Table 4 lists the various constants used in the simulation. The value of capacitors use parameters at 0 mm point from Fig. 5. A simulation is carried out using the above values. The output wave form of the inverter source uses a sine wave, and the load uses only pure resistance without a rectifier. Figs. 8 and 9 shows the output power using the series SS and parallel PS topologies, respectively, as well as input power factors, and show how the calculated value is reproduced approximately in the simulation. There are places where the values deviate in Fig. 8 at the time of constant input voltage and Fig. 9 at the time of constant input current. This may be due to loss caused by winding resistance, not considered by analysis, and/or due an error that increases as the total value of the coupling coefficient decreases.

Table 4. Simulation parameters

Gap[mm]	135
Frequency[kHz]	85
Load Resistance[Ω]	17
C_{s1},C_{s2}[μF](SS)	0.0214
C_{s3}[μF](SS)	0.0249
C_{p1},C_{p2}[μF](PS)	0.0214
C_s[μF](PS)	0.0261
V_{inmax}[V]	141.2
$I_{inSSmax}$[A]	5.0
$I_{inPSmax}$[A]	0.5

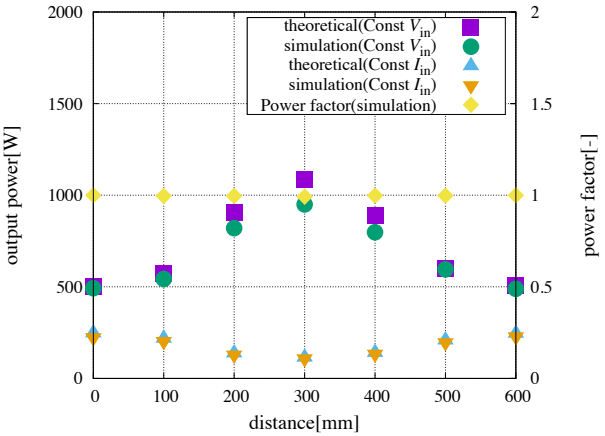

Fig.8 Output power of series SS topology(Simulation)

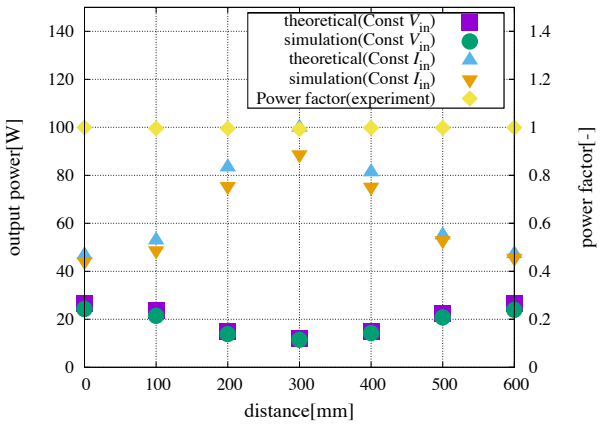

Fig.9 Output power of parallel PS topology(Simulation)

Table 5. Experiment parameters

Gap[mm]	135
Frequency[kHz]	85
DC Load Resistance R_d[Ω]	18.7
C_{s1},C_{s2}[μF](SS)	0.0217
C_{s3}[μF](SS)	0.0249
V_{in}[V]	100
I_{inSS}[A]	5.0

5. Experiment

An experiment is carried out to validate the equations calculated in Sections 3 and 4, with experimental verification limited to the

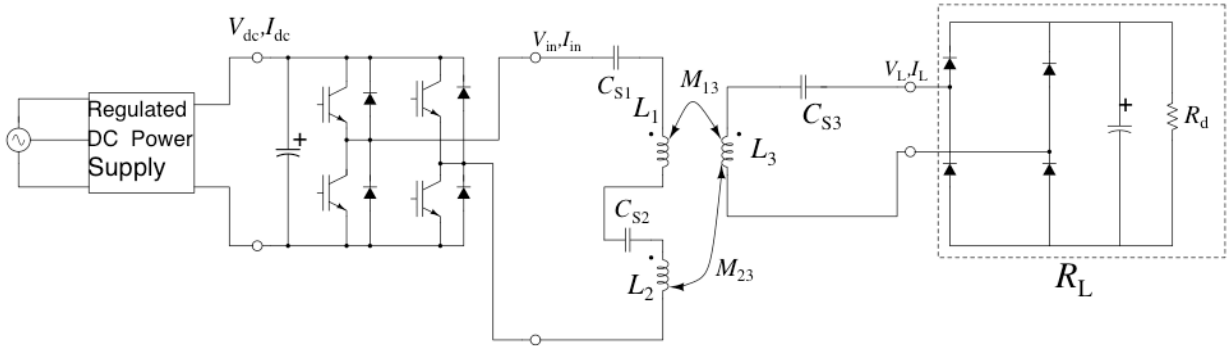

Fig. 10 Experiment circuit of series SS topology

series SS topology. Fig. 10 shows experiment circuit of SS topology. The experimental circuit is shown in Fig. 10. Additionally, Table 5 lists various constants used in the experiment. The input wave uses the RMS (square wave), converted between square wave voltage V_{inv} and fundamental wave voltage V_{in} , as

$$V_{in} = \frac{2\sqrt{2}}{\pi} V_{inv} . \tag{9}$$

Moreover, a load R_L uses a combination of DC electronic resistance and a full bridge rectifier. The conversion formula[8] is

$$R_L = \frac{8}{\pi^2} R_d . \tag{10}$$

The result for output power of the series SS topology is shown in Fig. 11. There is a large difference between the calculated theoretical values and the experimental values in Fig. 11 (a). They may be due to a variation of the power factor by an invisible factor during the analysis. The larger the change in values, the greater the influence of the power factor change becomes; the smaller the change in values, the smaller the influence of the power factor change. Nevertheless, the qualitative changes are in approximate agreement.

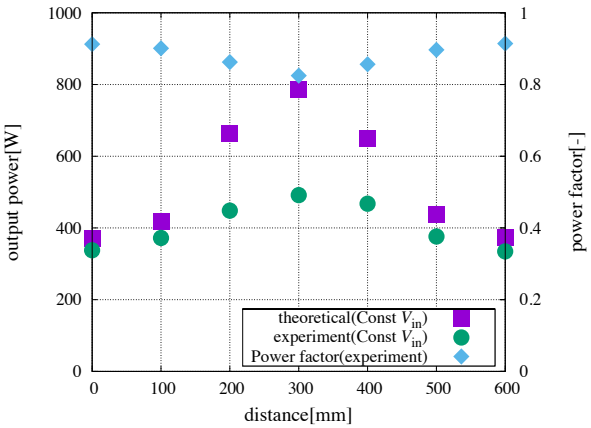

(a) constant V_{in}

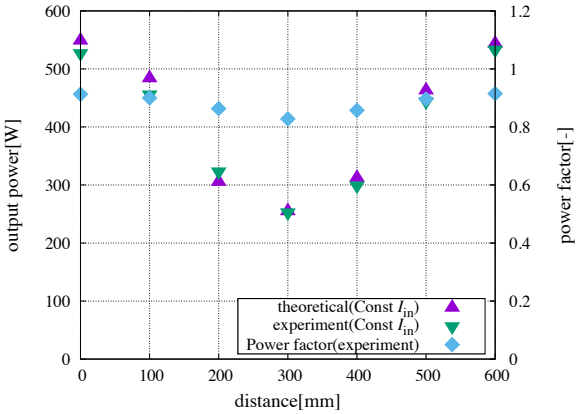

(b) constant I_{in}

Fig. 11 Output power of series SS topology(experiment)

6. CONCLUSION

This paper analyzes the input voltage and current, and the output voltage, current, and power of the series SS and the parallel PS topologies using two primary coils and a secondary coil, with a focus on the series SS topology for experimental verification. The trends of the theoretical equation and the circuit simulation value are in approximately agreement. There are places where the values deviate significantly when constant voltage is input, probably because of a variation of the power factor caused by an invisible factor in the analysis. In the future, this work will be extended to include experimental verification of the parallel PS topology, including parallel SS topology, i.e., parallel connection of primary coils in series to resonant capacitors, and perform a comparative analysis of the results on the series SS and parallel PS topologies. Moreover, it will analyze the impact of increasing the number of primary coils.

REFERENCES

(1) T.Yasuda, T. Fujita, and M, Sato , “Proposed dynamic contactless power transfer system,” in Proc. EVS28, 2015, vol. B5-02, pp. 1—6.

(2) Y. Chen, S. Park, J. Kim, H. Kim, K. Hwang, J. Kim, and S. Ahn, “System and electromagnetic compatibility of resonance coupling wireless power transfer in on-line electric vehicle,” -in Proc. ISAP, 2012, no. 1E3-1, pp. 158—161.

(3) K. K. Kim, T. Imura, and Y. Hori, “New wireless power transfer via magnetic resonant coupling for charging moving electric vehicle, ” in Proc. EVTeC and APE 2014, 2014, no. 20144026, pp. 1—5.

(4) T. Fujita, T. Yasuda, and H. Akagi, “A dynamic wireless power transfer system applicable to a stationary system,” IEEE Trans. Industry Applications, vol. 53, no 4, pp. 3748—3757, Jun. 2017

(5) J. Yamada, K Tsuda, R. Kobayashi, Y. Kaneko, “Circuit analysis and characterization of contactless power transfer system with variable impedance,” IEEJ Trans. Industry Applications, vol. 137 no.11, pp. 815—826, Nom. 2017 (in japanese)

(6) H.Irie and Y. Yamada, “Immittance converter suitable for power electronics,” Elect. Eng. Japan, vol. 124, no. 2, pp. 53—62, Jul. 1998

(7) C. Kato, K. Tsuda, T. Matsumura, Y. Kaneko, T. Fujita, and T. Yasuda, “Investigation of wireless power transfer system with spaced arranged primary H-shaped core coils for moving EVs,” in Proc. IEEE IECON 2015, 2015, pp.5197—5201.

(8) R. L. Steigerwald, “A comparison of half-bridge resonant converter topologies,” IEEE Trans. Power Electronics, vol. 3, no. 2, pp. 174—182, Apl. 1988